SCIENTIFIC REPORTS

OPEN

Received: 26 January 2016
Accepted: 31 March 2016
Published: 18 April 2016

# Bio-inspired cofacial Fe porphyrin dimers for efficient electrocatalytic $CO_2$ to CO conversion: Overpotential tuning by substituents at the porphyrin rings

Zaki N. Zahran[1,2], Eman A. Mohamed[1] & Yoshinori Naruta[1]

**Efficient reduction of $CO_2$ into useful carbon resources particularly CO is an essential reaction for developing alternate sources of fuels and for reducing the greenhouse effect of $CO_2$. The binuclear Ni, Fe—containing carbon monoxide dehydrogenase (CODHs) efficiently catalyzes the reduction of $CO_2$ to CO. The location of Ni and Fe at proper positions allows their cooperation for $CO_2$ to CO conversion through a push—pull mechanism. Bio—inspired from CODHs, we used several cofacial porphyrin dimers with different substituents as suitable ligands for holding two Fe ions with suitable Fe—Fe separation distance to efficiently and selectively promote $CO_2$ to CO conversion with high turnover frequencies, TOFs. The substituents on the porphyrin rings greatly affect the catalysis process. By introducing electron-withdrawing/-donating groups, e.g. electron-withdrawing perfluorophenyl, at all meso positions of the porphyrin rings, the catalysis overpotential, $\eta$ was minimized by ≈0.3 V compared to that obtained by introducing electron-donating mesityl groups. The Fe porphyrin dimers among reported catalysts are the most efficient ones for $CO_2$ to CO conversion. Control experiments indicate that the high performance of the current $CO_2$ to CO conversion catalysts is due to the presence of binuclear Fe centers at suitable Fe—Fe separation distance.**

The efficient reduction of $CO_2$ into useful carbon resources particularly CO is an essential reaction to overcome the limited supply of fossil fuels and the greenhouse effect of $CO_2$[1–3]. The $CO_2$ to CO reduction is, for example, useful for generating syngas ($CO + H_2$), which can be used to generate a wide variety of fuels with the current Fischer-Tropsch technologies[4]. Moreover, CO is a useful resource in methanol synthesis[5] and in hydroformylation[6]. Plenty of homogeneous or heterogeneous $CO_2$ to CO conversion catalysts have been reported. These include precious metal- (e.g. Re[7–11], Ru[12–15], Ir[16], Au[17,18], etc.) or non-precious metal- (e.g. Fe[19–23], Ni[24–26], Mn[27,28] etc.) based catalysts. For large-scale fuel production, the development of base metal catalysts is essential[29].

As base metal catalysts, Fe porphyrin monomers have been reported to efficiently catalyze the electrochemical reduction of $CO_2$ to CO in the presence of external or localized phenol as a weak proton donor to act as a proton relay during $CO_2$ to CO conversion. The electro-generated $Fe^0$ porphyrin undergoes a concerted proton-electron transfer bond cleavage (CPETBC: electron transfer from the central Fe atom concerted with proton transfer and breaking of one C-O bond) rate-determining step to form an Fe—CO species that undergoes further reduction to release CO[19–23].

In biological systems, several anaerobic bacteria and archaea utilize Ni, Fe—containing carbon monoxide dehydrogenases (CODHs) with a $[NiFe_4S_4]$ cluster at the active site as highly efficient catalyst for $CO_2$ to CO conversion with high turnover frequency, TOF (12 $s^{-1}$) at a low overpotential, $\eta < 100$ mV[30–36]. Binding to Ni and

[1]Institute for Science and Technology Research, Centre for Chemical Energy Conversion, Chubu University, Kasugai 487-8501, Japan. [2]Faculty of Science, Tanta University, Tanta, Egypt. Correspondence and requests for materials should be addressed to Z.N.Z. (email: znzahran@yahoo.com) or Y.N. (email: naruta@isc.chubu.ac.jp)

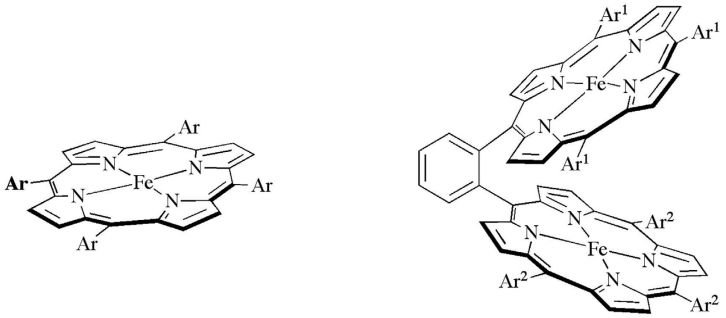

**FeTPFPP,** Ar = $C_6F_5$
**FeTF$_2$PP,** Ar = 2,6-$F_2C_6H_3$
**FeTCl$_2$PP,** Ar = 2,6-$Cl_2C_6H_3$
**FeTPP,** Ar = $C_6H_5$
**FeTMP,** Ar = 2,4,6-$Me_3C_6H_2$

**Fe$_2$DTPFPP,** $Ar^1$, $Ar^2$ = $C_6F_5$
**Fe$_2$DTF$_2$PP,** $Ar^1$, $Ar^2$ = 2,6-$F_2C_6H_3$
**Fe$_2$DTCl$_2$PP,** $Ar^1$, $Ar^2$ = 2,6-$Cl_2C_6H_3$
**Fe$_2$DTPP,** $Ar^1$, $Ar^2$ = $C_6H_5$
**Fe$_2$DTMP,** $Ar^1$, $Ar^2$ = 2,4,6-$Me_3C_6H_2$
**Fe$_2$TPFPP-TMP,** $Ar^1$ = 2,4,6-$Me_3C_6H_2$, $Ar^2$ = $C_6F_5$

**Figure 1. Chemical structures of the six Fe porphyrin dimers and their corresponding monomers.**

Fe activates $CO_2$ where Ni acts as a Lewis base to transfer a net electron to the antibonding lowest unoccupied molecular orbital of $CO_2$ that increases the negative partial charges at the oxygen atoms which are stabilized by binding to a Lewis acid Fe center[30–36]. The biological $CO_2$ to CO conversion indicates the importance of the binuclear metal ion centers with suitable separation distance in designing highly efficient catalysts for $CO_2$ to CO conversion. Indeed, $CO_2$ to CO conversion have been demonstrated with several binuclear- (e.g. $Ni_2$[37–39], $Cu_2$[40], $Ir_2$[41], and $Pd_2$[42]) and polynuclear- (e.g. $Ni_3$[43,44], $Fe_4$[45], and iron-sulfur clusters; $[Fe_4S_4(SR)_4]^{2-}$, Ni−$Fe_4S_4$ and Co−$Fe_4S_4$[46–48]) catalysts, however, with low TOF and/or high $\eta$-values.

Inspired from the Ni, Fe−containing CODHs, we recently reported a cofacial Fe tetraphenylporphyrin dimer, *o*-$Fe_2$DTPP having binuclear Fe centers at a suitable Fe−Fe separation distance that efficiently and selectively catalyzes the electrochemical $CO_2$ to CO conversion in a DMF/10% $H_2O$ solution with high Faradic efficiency (95%) and TOF (4,300 $s^{-1}$) without use of any acids. However, its reaction showed a relatively high overpotential, $\eta = 0.66$ V. Control experiments with the mononuclear Fe porphyrin monomer, FeTPP and the 1,3-phenylene bridged binuclear Fe porphyrin dimer, *m*-$Fe_2$DTPP indicate the importance of the binuclear Fe centers and the Fe−Fe separation distance for the $CO_2$ to CO conversion[49]. Here we introduced electron-donating and electron-withdrawing substituents to the peripheral porphyrin rings (Fig. 1) that tuned $\eta$ and the activity of the catalytic process. We also performed control experiments with Fe porphyrin monomers (Fig. 1) that show low activity for $CO_2$ reduction compared to that obtained with the binuclear Fe porphyrin dimers that clearly demonstrate the importance of the binuclear metal centers for the high activity and stability in designing $CO_2$ to CO conversion molecular catalysts. Benchmarking with other catalysts, the binuclear Fe porphyrin dimers are, to the best of our knowledge, the most efficient and stable homogeneous molecular catalysts for $CO_2$ to CO conversion at present.

## Results

Six porphyrin dimer ligands linked by a 1,2-phenylene bridge and bearing different substituents at the porphyrin rings have been prepared according to stepwise methods outlined in Scheme S1 (SI). Fe was then inserted into the porphyrin cavities by similar reported procedures[49]. Typically excess $FeBr_2$ was refluxed with the porphyrin dimer ligand in DMF overnight under Ar. The compounds were purified by column chromatography and characterized with ordinary spectroscopic methods including UV-vis., $^1$HNMR, and mass spectroscopy (Figure S1, SI). For control experiments, we also prepared their corresponding Fe porphyrin monomers.

In a DMF/0.1 M $^n$But$_4$NPF$_6$ ($^n$But$_4$NPF$_6$ = tetra-*n*-butylammonium hexafluorophosphate) solution saturated with Ar, the Fe porphyrin dimers (0.5 mM) and their corresponding Fe porphyrin monomers (1 mM) depict cyclic voltammetric (CV) behaviors shown in Figure S2 (SI) at a 50 mV/s scan rate. The Fe porphyrin monomers show, as previously reported[34–38], three successive reversible 1e$^-$ reductions/oxidations of the Fe centers, *i.e.* $Fe^{III/II}$, $Fe^{II/1}$ and $Fe^{I/0}$ at standard redox potentials donated as $E^0(1)$, $E^0(2)$, and $E^0(3)$, respectively. The Fe porphyrin dimers, on the other hand, show three successive 2e$^-$ reductions/oxidations of the two Fe centers represented by equations (1)~(6) at standard redox potentials donated as $E^0(1)$, $E^0(2)$, and $E^0(3)$ for $2Fe^{III/II}$, $2Fe^{II/1}$ and $2Fe^{I/0}$, respectively. In some cases, the 2e$^-$ reductions/oxidations process of the dimers are divided into two successive 1e$^-$ reductions/oxidations with standard redox potentials donated as, for example, $E^0$(1a) and $E^0$(1b). The number of electrons was confirmed by controlled-potential electrolysis carried out at 100 mV negative potentials of the peak potentials. Table S1 (SI) summarizes the standard redox potentials, $E^0$, of the Fe porphyrin dimers and their corresponding Fe porphyrin monomers *vs.* NHE (hereafter, all potentials are indicated against NHE

except as noted). The standard redox potential of the $2Fe^{III/II}$ reductions/oxidations of the dimers, $E^0(1)$ occur at significant negative potentials relative to that of the monomer possibly due to strong $Cl^-$ binding/association to the Fe centers between the two cofacial porphyrin bi-layers[49]. The peak currents of the Fe porphyrin dimers are significantly smaller than that of the corresponding Fe porphyrin monomers. This is consistent with their small diffusion coefficients resulting from their large molecular sizes relative to their corresponding Fe porphyrin monomers[50]. The reduction peak currents of the Fe porphyrin dimers change linearly with the square root of the scan rate, $\upsilon^{1/2}$ indicating diffusion controlled electron transfer processes[50]. The standard redox potentials, $E^0$, reflect the different electronic environment around the Fe centers. For example, $E^0$s are shifted to more positive potentials as the electron-withdrawing properties of the substituents on the peripheral porphyrin rings increase. Also, a clear separation among $E^0(1a)$ and $E^0(1b)$, $E^0(2a)$ and $E^0(2b)$, and $E^0(3a)$ and $E^0(3b)$ couples were observed for the $Fe_2$TPFPP-TMP dimer that has a significant difference in the electronic environment around the two Fe centers.

$$[Fe^{III}Fe^{III}]^{2+} + e^- \xrightarrow{E^0(1a)} [Fe^{II}Fe^{III}]^+ \quad (1)$$

$$[Fe^{II}Fe^{III}]^+ + e^- \xrightarrow{E^0(1b)} [Fe^{II}Fe^{II}]^0 \quad (2)$$

$$[Fe^{II}Fe^{II}]^0 + e^- \xrightarrow{E^0(2a)} [Fe^{I}Fe^{II}]^- \quad (3)$$

$$[Fe^{I}Fe^{II}]^- + e^- \xrightarrow{E^0(2b)} [Fe^{I}Fe^{I}]^{2-} \quad (4)$$

$$[Fe^{I}Fe^{I}]^{2-} + e^- \xrightarrow{E^0(3a)} [Fe^{0}Fe^{I}]^{3-} \quad (5)$$

$$[Fe^{0}Fe^{I}]^{3-} + e^- \xrightarrow{E^0(3b)} [Fe^{0}Fe^{0}]^{4-} \quad (6)$$

Under $CO_2$, the CV behaviors of the Fe porphyrin dimers (0.5 mM) are depicted in Fig. 2 (red lines). The reversible $2Fe^{III}/2Fe^{II}$ redox couple observed under Ar is replaced with a new reduction peak due, as we previously reported[49], to the dissociation of the $Cl^-$ and the coordination of the $CO_2$ molecule to the electro-generated $2Fe^{II}$ species inside the cofacial porphyrin cavity within the time scale of CV. The dissociation of the $Cl^-$ and coordination of $CO_2$ is supported by the UV-vis spectra of the chemically reduced *o*-$Fe_2^{II}$DTPP that shows the remarkable change of its Soret and Q-bands upon purging of $CO_2$ gas at −30 °C, indicating the binding of $CO_2$ to the $Fe^{II}$ porphyrin species[49]. Indeed, the ability of $CO_2$ to coordinate transition metal complexes is extensively investigated[51]. However, the coordination of $CO_2$ to the electro-generated $Fe^{II}$ species is not observed in the corresponding Fe porphyrin monomer under similar experimental conditions. Upon further scanning to more negative potential the electro-generated $CO_2$-coordinated $2Fe^{II}$ species showed a reversible $2e^-$ redox couple corresponding to the generation of $CO_2$ coordinated $2Fe^{II}/2Fe^{I}$ species. The most interesting finding is the observation of a strong catalytic current in the presence of $CO_2$ indicating electro-catalytic reduction of $CO_2$ promoted by the six Fe porphyrin dimers. The appearance of the catalytic peak over the $Fe^IFe^I/Fe^IFe^0$ redox couple under Ar indicates the starting of the catalytic process once the $Fe^IFe^0$ porphyrin species is electrochemically generated[49]. In general, the Fe porphyrin dimer with electron-withdrawing substituents shows electro-catalytic $CO_2$ reduction behavior at more positive potential, i.e. at low $\eta$. In other words, the Fe porphyrin dimers are arranged in the following order with respect to their $\eta$ (small to large) for the $CO_2$ to CO conversion; $Fe_2$DTPFPP < $Fe_2$TPFPP-TMP < $Fe_2$DTF$_2$PP < $Fe_2$DTCl$_2$PP < $Fe_2$DTPP < $Fe_2$DTMP.

The effect of $H_2O$ content on the catalytic $CO_2$ to CO conversion with Fe porphyrin dimers is tested by CVs at a 100 mV/s scan rate. Figure S3 (SI) shows the CVs of *o*-$Fe_2$DTPP (0.5 mM) as a representative example at 100 mV/s scan rate in DMF containing 0.1 M $^n$But$_4$NPF$_6$ supporting electrolyte in the presence of different amounts of $H_2O$ under Ar or $CO_2$. All the other Fe porphyrin dimers show similar behaviors. In $H_2O$-free DMF solution, a large catalytic current was generated in a $CO_2$-saturated solution. Increasing the $H_2O$ content to 10% in the medium induces the positive shift of the starting potential of the catalytic current and increases the catalytic peak current, Further addition of $H_2O$ above 10% decreases the catalytic peak current due to the decreasing solubility of the Fe porphyrin dimers.

For fast catalytic process, the foot-of-the-wave analysis of the CVs has been reported to be a quick estimation of the catalysis rate constant, $k_{cat}$, TON, and TOF of the catalysis reaction without the contribution of side phenomena such as substrate consumption, catalyst deactivation, and/or product inhibition[19,23]. The analysis is based on the linear correlation between $i/i^0_p$ and $1/\{1 + \exp[F/RT(E - E^0_{cat})]\}$ "equation (7)",where $i$ is the catalytic current in the presence of $CO_2$, $i^0_p$ is the peak current in the absence of $CO_2$, $F$, $R$, $T$, and $E$ are the Faraday constant, gas constant, absolute temperature, and the electrode potential, respectively. Plotting $i/i^0_p$ *vs.* $1/\{1 + \exp[F/RT(E - E^0_{cat})]\}$ gives rise to a straight line of slope $2.24(RT/F\nu)^{1/2}(k_{cat})^{1/2}$ ($\nu$ is the scan rate in V/s) from which the catalysis rate constant, $k_{cat}$ is calculated. The $k_{cat}$ is then used to calculate the TOF and the logTOF $-\eta$ relationship according to equations (8) and (9), respectively, where $TOF^0$ is the intrinsic turnover frequency (turnover frequency at zero $\eta$). The value of $\eta$ is calculated according to equation (10) based on the reported thermodynamic redox potential of the $CO_2$ to CO conversion in DMF/5% $H_2O$ solution containing 0.1 M $^n$But$_4$NPF$_6$ supporting electrolyte, $E^0(CO_2/CO) = -0.69$ V[19]. Figure 3 depicts the catalytic CVs responses (left) of three Fe porphyrin dimers (0.5 mM, 100 mV/s scan rate) and the corresponding foot-of-the-wave analysis (right). Other

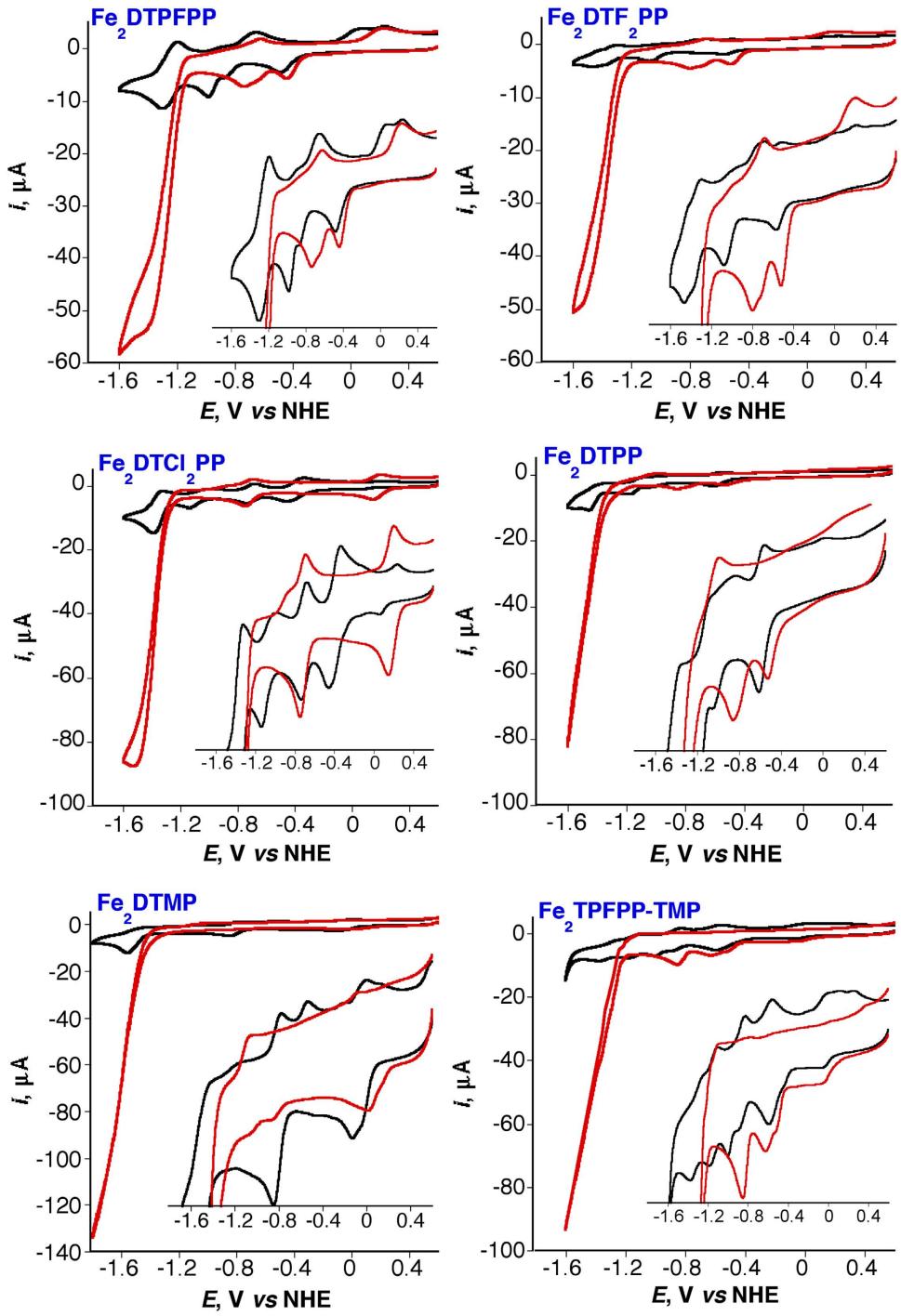


**Figure 2. Cyclic voltammograms of the six Fe-porphyrin dimers (0.5 mM) in DMF/10% $H_2O$ at 50 mV/s scan rate under Ar (black lines) and $CO_2$ (red lines).** Insets: magnified traces of CVs.

catalysts show similar behaviors. Figure 4 shows the catalytic CVs responses (a) of the six Fe porphyrin dimers and the corresponding logTOF $-\eta$ relationship (b). Table 1 summarizes the catalysis parameters of the current Fe porphyrin dimers and that of the most efficient reported $CO_2$/CO reduction molecular catalysts. The table clearly shows that $\eta$ for the $CO_2$ reduction decrease by increasing the electron-withdrawing substituents on the porphyrin rings for the Fe porphyrin dimers and their benchmarking superiority for the $CO_2$ to CO conversion activity over the reported catalysts.

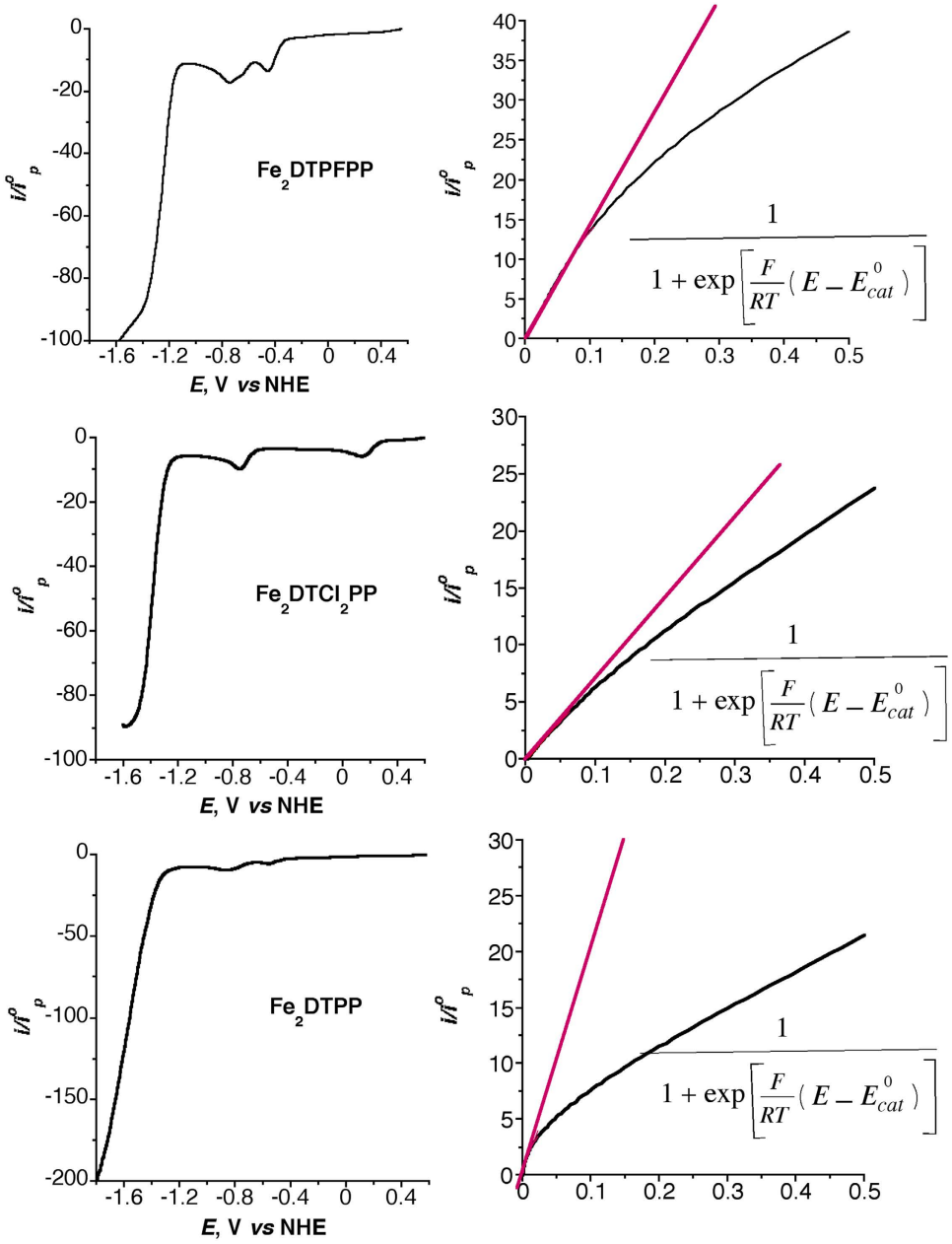


**Figure 3. Catalytic CV responses (left, forward scan only shown for clarity) of three Fe porphyrin dimers (0.5 mM) at 100 mV/s scan rate in DMF/10% $H_2O$ saturated with $CO_2$ and the corresponding foot-of-the-wave analysis (right).**

$$\frac{i}{i_p^0} = 2.24\sqrt{\frac{RT}{F\upsilon}k_{cat}}\frac{1}{1+\exp\left[\frac{F}{RT}(E-E_{cat}^0)\right]} \tag{7}$$

$$\mathrm{TOF} = \frac{k_{cat}}{1+\exp\left[\frac{F}{RT}(E-E_{cat}^0)\right]} \tag{8}$$

$$log\mathrm{TOF} = logk_{cat} - F/RTln10\left(E_{\mathrm{CO_2/CO}}^0 - E_{cat}^0\right) + F\eta/RTln10 \tag{9}$$

$$log\mathrm{TOF}^0 = logk_{cat} - F/RTln10\left(E_{\mathrm{CO_2/CO}}^0 - E_{cat}^0\right)$$

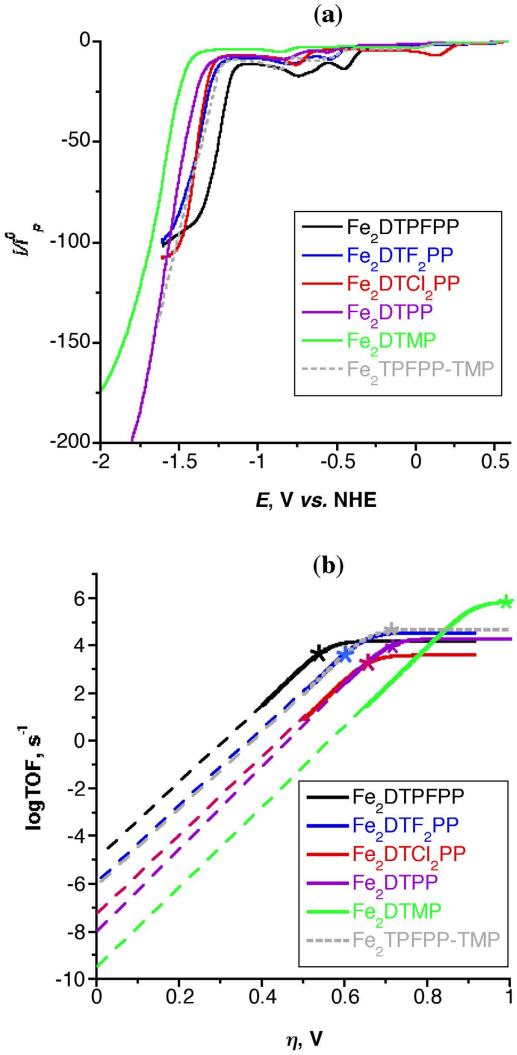


**Figure 4.** (**a**) Catalytic CVs responses (forward scan only shown for clarity) and (**b**) the Tafel plot [logTOF $-\eta$ relationships] of the six Fe porphyrin dimers (0.5 mM) at 100 mV/s scan rate in DMF/10% $H_2O$ saturated with $CO_2$. *logTOF resulted from bulk electrolysis experiments.

$$\eta = E - E^0_{CO_2/CO} \quad E^0_{CO_2/CO} = -0.69V \tag{10}$$

To test the activity, stability, and selectivity of the Fe porphyrin dimers for the $CO_2$ reduction, a bulk electrolysis experiment was conducted in a gas-tight H shaped two-compartment electrochemical cell with a glass frit to separate the two compartments. The cell was filled with DMF/10% $H_2O$ solution (14 mL) containing 0.5 mM of the Fe porphyrin dimer and 0.1 M $^n$But$_4$NPF$_6$ as a supporting electrolyte. In one compartment, a glassy carbon working electrode (1 $cm^2$) and a Ag/AgCl (3M NaCl) reference one were immersed close to each other (about 2 mm apart) in the solution. In the other compartment, a Pt foil (about 20 $cm^2$) was immersed in the solution and used as a counter electrode. The solution in the two compartments was saturated with $CO_2$ by bubbling $CO_2$ for 30 min prior to the reaction. The products of the electro-catalytic reduction in the gas phase and in the solution phase were analyzed by gas chromatography and capillary electrophoreses, respectively. Figure 5a shows the current density-time profile of the electrolysis at $-1.25$ V *vs.* NHE ($\eta = 0.56$ V) in the presence and absence of the $Fe_2$DTPFPP (0.5 mM) as a representative example of the Fe porphyrin dimers. The product analysis (Fig. 5b) of the headspace gas and solution shows the formation of CO gas in 92% Faradaic efficiency and $H_2$ gas in 8% Faradaic efficiency. Only a very small amount of $HCO_2H$ detected in the solution, that means the $Fe_2$DTPFPP dimer shows a high selectivity for $CO_2$ reduction to CO. The other Fe porphyrin dimers show similar behavior for the $CO_2$ to CO conversion however under slightly higher $\eta$. Based on the bulk electrolysis experiment, the catalysis parameters, $k_{cat}$, TON, and TOF were calculated using equations (11)~(13);

$$\frac{I}{F} = \frac{(k_{cat}D_{cat})^{1/2}C^0_{cat}}{1 + \exp(F/RT)(E - E^0_{cat})} \tag{11}$$

| Solvent $E^0(CO_2/CO)$, V | Catalyst $E^0_{cat}$,V | $k_{cat}$, $s^{-1}$ | $\eta$, V | logTOF, $s^{-1}$ | logTOF$^0$, $s^{-1}$ | Ref. |
|---|---|---|---|---|---|---|
| DMF/10% $H_2O$ −0.69 | $Fe_2$DTPFPP, −1.25 | $1.6 \times 10^4$ | 0.40 − 0.60 | 1.5 − 3.9, 4.2* | −5.0 | This work |
| DMF/10% $H_2O$ − 0.69 | $Fe_2DTF_2PP$, −1.34 | $3.7 \times 10^4$ | 0.50 − 0.65 | 2.0 − 4.3, 4.5* | −6.1 | This work |
| DMF/10% $H_2O$ − 0.69 | $Fe_2DTCl_2PP$, −1.35 | $4.1 \times 10^3$ | 0.55 − 0.70 | 1.8 − 3.5, 3.6* | −7.2 | This work |
| DMF/10% $H_2O$ − 0.69 | $Fe_2$DTPP, −1.40 | $2.0 \times 10^4$ | 0.60 − 0.75 | 2.4 − 4.2, 4.3* | −8.1 | This work[49] |
| DMF/10% $H_2O$ − 0.69 | $Fe_2$DTMP, −1.60 | $4.1 \times 10^3$ | 0.70 − 0.85 | 2.3 − 4.8, 5.8* | −9.6 | This work |
| DMF/10% $H_2O$ − 0.69 | $Fe_2$TPFPP, −TMP −1.35 | $7.3 \times 10^5$ | 0.55 − 0.70 | 2.8 − 4.3, 4.7* | −6.1 | This work |
| DMF/10% $H_2O$ − 0.69 | FeTPP, − 1.41 | $2.1 \times 10^3$ | 0.60 − 1.0 | 1.4 − 3.1, 3.3* | −8.4 | This work |
| DMF/5% $H_2O$ /3M PhOH −0.69 | CAT[a], − 1.35 | $>5.0 \times 10^6$ | 0.45 − 0.70 | 1.8 − 3.2, 3.8* | −6.0 | 22 |
| DMF/5% $H_2O$ /3M PhOH −0.69 | FCAT[b], − 1.28 | $>5.0 \times 10^6$ | 0.40 − 0.70 | 1.6 − 3.8, 4.0* | −5.5 | 22 |
| DMF/5% $H_2O$ /3M PhOH −0.69 | FeTPP, −1.43 | $3.5 \times 10^4$ | 0.60 − 1.00 | 2.5 − 4.3, 4.5* | −8.0 | 20 |
| $CH_3CN$/0.8M $CF_3CH_2OH$ −0.65 | Re(bpy)(py)$(CO)_3$, −1.30 | 875.0 | NA | 2.9* | −8.0 | 11 |
| $CH_3CN$ −0.65 | (bbpy)Mn$(CO)_3$, −1.28 | $5.0 \times 10^3$ | NA | 3.7* | −7.0 | 28 |
| $CH_3CN$ −0.65 | Ru(tpy)(Mebim-py), −1.34 | 59.0 | NA | 1.8* | −9.9 | 12 |
| $CH_3CN$ −0.65 | Ru(tpy)(bpy) −1.34 | 7.6 | NA | 0.9* | −10.8 | 12 |
| DMF/0.1M $HBF_4$ −0.23 | *m*-(triphos)$_2Pd_2$, −0.76 | 35.0 | NA | 1.5* | −7.4 | 42 |

**Table 1. Catalysis parameters of Fe porphyrin dimers (this work) and other reported molecular $CO_2$/CO reduction catalysts.** [a]Fe *meso*-tetra(2,6-dihydroxyphenyl)porphyrin. [b]Fe 5,15-di((2,6-dihydroxyphenyl)-10,20-di(pentafluorophenyl)porphyrin. *logTOF$_{max}$, $s^{-1}$.

$$\mathrm{TOF} = \frac{k_{cat}}{1 + \exp[F/RT\,(E - E^0_{cat})]} \tag{12}$$

$$\mathrm{TON} = \frac{k_{cat}t}{1 + \exp[F/RT\,(E - E^0_{cat})]} \tag{13}$$

where, $I$ is the net current density (the current density obtained from the bulk electrolysis corrected for the background current density and Faradic efficiency), $D_{cat}$ is the diffusion coefficient of the catalyst calculated based on Randles-Sevcik equation[50], and $C^0_{cat}$ is the bulk catalyst concentration, $5 \times 10^{-7}$ mole/cm$^3$ (0.5 mM). Table S2 (SI) summarizes the catalysis parameters of the six Fe porphyrin dimers obtained from the bulk electrolysis experiment conducted for 6 hrs in DMF/10% $H_2O$ saturated with $CO_2$. The results of the bulk electrolysis experiments conducted at a single potential are presented as stars in Fig. 4b that demonstrate the validity of the foot-of-the-wave analysis for estimating the catalysis parameters[19].

To clarify the indispensableness of the dimer structure for the high catalytic activity as $CO_2$ to CO conversion catalysts as well as to compare the catalytic performance between the dimers and the monomers, we prepared the corresponding Fe porphyrin monomers, FeTPFPP, $FeTF_2PP$, $FeTCl_2PP$, FeTPP and FeTMP (Fig. 1) as controls and measured their CV behaviors under Ar or $CO_2$ in DMF/10% $H_2O$ solution. To normalize for the concentration of their iron centers, the Fe porphyrin monomers and dimers were tested at 1 mM and 0.5 mM concentration, respectively. Under Ar (Figure S2, SI), the Fe porphyrin monomers show three reversible 1e$^-$ redox couples assigned for the $Fe^{III/II}$, $Fe^{II/I}$, and $Fe^{I/0}$ at standard redox potentials depicted in Table S1. Under $CO_2$, the Fe porphyrin monomers show catalytic current peaks for the $CO_2$ reduction, however, lower than those shown by the corresponding Fe porphyrin dimers. This indicates the importance of the binuclear Fe centers for the high activity of the current Fe porphyrin dimers as $CO_2$ to CO conversion catalysts. Figure S4 (SI) shows the CVs of the $Fe_2$DTPFPP and FeTPFPP under Ar and $CO_2$ as, a representative example, which clearly shows the high activity of the Fe porphyrin dimer compared to the corresponding monomer for $CO_2$ to CO conversion without use of any acids.

For a clear kinetic comparison between the Fe porphyrin dimers and their corresponding monomers for $CO_2$ to CO conversion, the catalytic peak current, $i$ is normalized to the peak current of the $Fe^{II/I}$, $i^0_p$. Figure S5 (SI) compares the activity of the six Fe porphyrin dimers with their corresponding monomers. Table S3 (SI) summarizes the catalysis parameters of the Fe porphyrin monomers, derived from the foot-of-the-wave analysis of the CVs. These results clearly elucidate that the binuclear structure is essential for highly efficient $CO_2$ reduction. We tentatively propose that the cofacial dimer structure will provide a suitable way for the cooperation of the two Fe centers during the $CO_2$ electro-catalytic reduction similar to that observed in CODHs. Consistent with this, the 1,3-phenylene bridged Fe porphyrin dimer, *m*-$Fe_2$DTPP that has a large Fe-Fe separation distance (≈10.9 Å) showed very low activity (Table S3) for $CO_2$ to CO conversion compared with the current cofacial Fe porphyrin dimers under the same conditions[49].

## Discussion

In biological systems, CODHs use a $[NiFe_4S_4]$ cluster, termed cluster C, to reversibly reduce $CO_2$ to CO with high TON and TOF at low $\eta$. The crystallographic studies, at the atomic resolution (≤1.1 Å) of CODH in complex with $CO_2$ revealed a $CO_2$ ligand bridged between Ni and Fe in a $\mu_2\eta^2$ coordination geometry that clearly indicates the cooperation between the binuclear Ni and Fe centers in the activation of $CO_2$ reduction[36]. The presence of

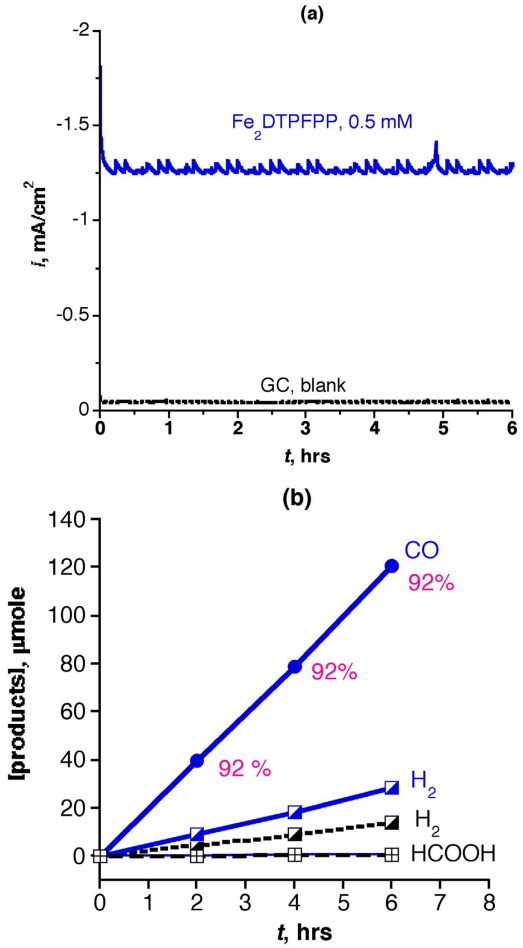


**Figure 5.** (**a**) Bulk electrolysis conducted for 6 hrs at −1.25 V *vs.* NHE ($\eta = 0.56$ V) and (**b**) products analysis of $Fe_2$DTPFPP (0.5 mM) and GC blank in DMF/10% $H_2O$ under $CO_2$.

binuclear Ni and Fe centers in CODHs inspired us to utilize molecular inorganic catalysts containing binuclear centers for $CO_2$ to CO conversion keeping in mind that the binuclear centers should be at a suitable separation distance to allow the cooperation between them. We previously utilized several cofacial porphyrin dimers as suitable ligands for holding two Mn ions at suitable Mn−Mn separation distances (3.7–6.2 Å) to promote water oxidation to $O_2$ or $H_2O_2$ disproportionation[52–54]. As a first generation of molecular catalysts containing binuclear centers, we utilized six cofacial porphyrin dimers ligands with different electron donating and withdrawing substituents at the peripheral porphyrin rings and holding two Fe ions as bio-inspired catalysts for $CO_2$ to CO conversion. Assuming similar Fe−Fe separation distances in the current catalysts, this will fit $CO_2$ bridging to the Fe ions and allowing their cooperation for the $CO_2$ to CO conversion. The results obtained demonstrate that, the Fe porphyrin dimers have the greatest activity, stability, and selectivity for $CO_2$ electro-catalytic reduction to CO among the reported precious and non-precious $CO_2$ to CO reduction molecular catalysts (Table 1). Control experiments with Fe porphyrin monomers (Figure S2, Table S3) and a 1,3-phenylene bridged Fe porphyrin dimer (Table S3) indicate the importance of the binuclear Fe centers and the Fe−Fe separation distance for the high catalytic performance.

On the time scale of CV, the data show that the cofacial Fe porphyrin dimers under Ar are reduced stepwisely as in equations (1)~(6). Under $CO_2$, the catalytic current for the $CO_2$ to CO conversion is observed on the peaks corresponding to $[Fe^IFe^I]$ to $[Fe^IFe^0]$ and $[Fe^IFe^0]$ to $[Fe^0Fe^0]$ conversions as in equations (5) and (6) (Fig. 2). This means the active species for the $CO_2$ reduction is either $[Fe^IFe^0]$ or $[Fe^0Fe^0]$ species. The differentiation between the two species is unclear in the five symmetrical Fe porphyrin dimers where the two Fe centers have similar electronic environments. The hetero-dimer, $Fe_2$TPFPP-TMP that has quite different electronic environment around the two Fe centers, on the other hand, showed clear separation of the stepwise reductions of the Fe centers under Ar (Table S1) and showed only strong catalytic current over the $[Fe^IFe^0]$ species (Fig. 2) under $CO_2$. This observation indicates that $Fe^0$ and $Fe^I$ possibly act as a Lewis base and a Lewis acid, respectively, in the catalysis process. Through such roles of the binuclear centers, these Fe porphyrin dimers would promote the $CO_2$ reduction without any acids[49]. At its lower reduced state, $Fe^{II}Fe^{II}$, these catalysts can capture $CO_2$, judging from the appearance of a new CV peak under $CO_2$ atmosphere (Fig. 2)[49]. This association of substrate $CO_2$ and the catalysts at the lower reduced state will contribute to the increase of TOF in the dimer catalysts, because it is ready to do the rapid reduction of the bound $CO_2$ at the catalyst $Fe^0Fe^I$ state.

The results obtained by the current cofacial Fe porphyrin dimers also indicate that $\eta$ and TOF of the catalysis process can be tuned by the introduction of electronically different substituents to the porphyrin peripheral positions (Fig. 4 and Table 1). For example, introduction of electron-withdrawing perfluorophenyl substituents to the meso positions of the dimer reduces $\eta \approx 0.3$ V compared to that obtained with electron-donating mesityl group. In general, the introduction of electron-withdrawing groups on catalysts promotes the positive shifts of their reduction potentials, resultantly decrease of $\eta$ of the reduction reaction. However, this electron-withdrawing effect also causes the decrease of the electron density at the active center, which sacrifices their nucleophilic activities to lead the decrease of TOF. On the other hand, electron-donating groups such as mesityl on the porphyrin rings leads high TOFs. In general, low reaction $\eta$ and high TOF by electronic tuning is not compatible[22], although TOFs for the dimer catalysts are kept within the moderate range even the catalysts bearing electron-withdrawing groups.

This work will turn the intention for designing new generations of highly efficient binuclear molecular catalysts for $CO_2$ to CO conversion, working under neutral conditions. We are currently trying to obtain hetero-binuclear dimers to elucidate the catalytic mechanism.

## Methods

Materials, Instruments, CV measurements, Bulk electrolysis, and products analysis of $CO_2$ reduction are presented in the supporting information.

**Preparation of Fe porphyrin dimers.** The cofacial Fe porphyrin dimers were prepared as previously reported by stepwise procedures according to Scheme S1 (SI)[49,55]. We will discuss the preparation of [$Fe_2$DTMP]$Cl_2$ as a representative example in details. The other dimers were synthesized similarly.

**Preparation of 5-(2′-methylbenzoate)-10,15,20-trismesityl-porphyrin (compound b, $Ar^1 = 2,4,6\text{-}Me_3C_6H_2$).** A 2 L three-neck round-bottomed flask was charged with Methyl-2-formylbenzoate (**a**) (1.94 mL 11.8 mmol), mesitylaldehyde (4.5 mL, 36 mmol), pyrrole (3.2 mL, 48 mmol) and $CHCl_3$ (600 mL). The colorless solution was purged with nitrogen for about 15 min. Then, boron trifluoride diethyl etherate ($BF_3{\cdot}Et_2O$, 3.2 mL) was added via a syringe, accordingly the color of the solution changed immediately to dark red. The mixture was stirred at room temperature under nitrogen and TLC used to monitor the reaction progress. At the end of 5-hrs. reaction, DDQ (DDQ = 2,3-dichloro-5,6-dicyano-*p*-benzoquinone) solution (8 g/150 mL benzene, 36 mmol) was added to the reaction mixture, whose color changed to dark green. The mixture was stirred at room temperature for 1.5 hours. After solvent removal, the residue was dissolved into a small amount of $CHCl_3$ and loaded into $Al_2O_3$ column then eluted with $CHCl_3$. The first broad reddish violet band was collected. The TLC of this band showed the presence of three bands; a light red band on the top followed by strong reddish violet band then green and black bands on the bottom. The mixture was separated by a silica-gel column. The first red band eluted with *n*-hexane-benzene mixture (1:1 v/v) was collected and characterized as 0.2 g $TMPH_2$ byproduct. The second reddish violet band contained 1.6 g of the desired compound b. The compound was further purified with a silica-gel column eluted with *n*-haxane- $CHCl_3$ (1:1 v/v) to give the pure one (1.4 g, 14.8% yield). $^1$H NMR ($CDCl_3$, 400 MHz): δ 8.65 (d, 8H, pyrrole β-H), 8.39 (m, 1H, Ar-H), 8.09 (m, 1H, Ar-H), 7.85 (m, 2H, Ar-H), 2.86 (s, 3H, $OCH_3$), 2.64 (s, 9H, Ar-$CH_3$), 2.00 (s, 3H, Ar-$CH_3$), 1.88 (s, 3H, Ar-$CH_3$), 1.86 (s, 9H, Ar-$CH_3$), 1.80 (s, 3H, Ar-$CH_3$), −2.46 (s, 2H, pyrrole N-H). MALDI-TOF-MS *m/z* = 798.25 (found), 799.02 (calcd.).

**Preparation of 5-(2′-Benzomethanol)-10,15,20-mesitylporphyrin (compound c).** A 500 mL flask was charged with compound **b** (0.5 g, 0.626 mmol) and dry THF (15 mL). The solution was cooled to 0 °C then LDBBA (LDBBA = lithium diisobutyl-*t*-butoxyaluminum hydride) reducing agent (12.5 ml, 4 mmol, 0.33 M solution) was added drop-wise. The reaction mixture was stirred for 3 hrs at 0 °C under $N_2$ while its progress was monitored with TLC. After completed, the reaction quenched by adding 2M HCl and the product was extracted three times with $CH_2Cl_2$. The solvent was removed and the residue was purified with a silica-gel column using $CH_2Cl_2$ as an eluent to give a pure violet powder of the desired compound (0.47 g, 97.5% yield). $^1$HNMR ($CDCl_3$, 400 MHz): δ 8.62 (d, 8H, pyrrole β-H), 8.02 (m, 1H, Ar-H), 7.93 (m, 1H, Ar-H), 7.82 (m, 1H, Ar-H), 7.63 (m, 1H, Ar-H), 4.38 (s, 2H, -$CH_2$OH), 4.05 (s, 1H, -OH), 2.57 (s, 9H, Ar-$CH_3$), 2.04 (s, 3H, Ar-$CH_3$), 1.96 (s, 3H, Ar-$CH_3$), 1.84 (s, 9H, Ar-$CH_3$), 1.53 (s, 3H, Ar-$CH_3$), −2.47 (s, 2H, pyrrole N-H). MALDI-TOF-MS *m/z* = 771.1 (found), 771.0 (calcd.).

**Preparation of 5-(2′-Benzaldehyde)-10,15,20-trismesityl-porphyrin (compound d).** Compound c (3.5 g, 4.5 mol) was dissolved into dry $CH_2Cl_2$ (500 mL) then excess active $MnO_2$ (~15 g) was added. The solution was stirred under $N_2$ for 2 hrs. The TLC showed complete conversion of the compound to d. The $MnO_2$ was isolated by filtration. The solvent was removed under vacuum and the residue was purified with Silica-gel column using $CH_2Cl_2$ as eluent to give a pure violet powder of the desired compound (3.2 g, 91.6% yield). $^1$H NMR ($CDCl_3$, 400 MHz): δ 8.66 (d, 8H, pyrrole β-H), 8.41 (m, 1H, Ar-H), 8.20 (m, 1H, Ar-H), 7.91 (m, 2H, Ar-H), 5.3 (s, 1H, -CHO), 2.62 (s, 9H, Ar-$CH_3$), 1.87 (s, 18H, Ar-$CH_3$), −2.52 (s, 2H, pyrrole N-H). MALDI-TOF-MS *m/z* = 768.5 (found), 768.99 (calcd.).

**Preparation of 1′,2′-bis[10,15,20-trimesitylporphyrin]-benzene (compound e).** A 1L three-necked flask was charged with compound d (2.0 g, 2.6 mmol), pyrrole (1.4 g, 20.8 mmol), mesitylaldehyde (3.05 g, 15.5 mmol), and dry $CH_2Cl_2$ (400 mL). The solution was stirred at room temperature for 30 min. under $N_2$. Then, $BF_3{\cdot}Et_2O$ catalyst (5 mL) was added. After 4-hrs stirring, DDQ solution (5 g in 100 mL benzene) was added and the stirring is continued for 2 more hrs. The solvent was reduced by the rotary evaporator and loaded to $Al_2O_3$ column and the porphyrins mixture was collected using $CHCl_3$ as eluent. The porphyrins mixture ($TMPH_2$ and the dimmer) was separated by using silica-gel column eluted with $CHCl_3$:hexane (1:3 v/v). The $TMPH_2$ came first

then the desired compound. The compound **e** was isolated as pure violet powder (0.85 g, 21% yield). $^1$H NMR ($CDCl_3$, 400 MHz): δ 9.04 (d, 4H, pyrrole β-H), 8.73 (dd, 2H, Ar-H), 8.19 (d, 4H, pyrrole β-H), 8.19–8.15 (m, 2H, Ar-H), 8.11 (d, 4H, pyrrole β-H), 7.93 (d, 4H, pyrrole β-H), 7.02 (s, 2H, Ar-H), 7.01 (s, 4H, Ar-H), 6.99 (s, 2H, Ar-H), 6.76 (s, 4H, Ar-H), 2.55 (s, 18H, Ar-$CH_3$), 1.47 (s, 36H, Ar-$CH_3$), −3.52 (s, 4H, por-pyrrole NH). MALDI-TOF-MS $m/z$ = 1547.2 (found), 1547.46 (calcd.).

**Preparation of diiron 1′-[10,15,20-trispentafluorophenyl-porphyrin]-2′-[10,15,20-trismesitylporphyrin]-benzene ($Fe_2$DTMP, Compound f).** A solution of compound e (200 mg, 0.13 mmol) in dry DMF (20 mL) was refluxed overnight with excess $FeBr_2$ (150 mg, 0.69 mmol). The solvent was then removed and the desired compound was extracted with $CHCl_3$/1M HCl three times then with $CHCl_3$/$NaHCO_3$ (saturated) in three times and finally with the $CHCl_3/H_2O$ in three times. The organic layer containing the desired compound was dried over anhydrous sodium sulfate. The compound was further purified with a silica-gel column using 5% MeOH-$CHCl_3$ as an eluent. The reddish brown band was collected to give reddish brown powder (197 mg, 88.3% yield). MALDI-TOF-MS $m/z$ = 1511, 1546, 1583 corresponding to $Fe_2$DTMP (calcd 1511.5), [$Fe_2$DTMP]Cl (calcd. 1546.95) and [$Fe_2$DTMP]$Cl_2$ (calcd. 1582.4), respectively.

Similarly, the other Fe porphyrin dimers were prepared and characterized by MALDI-TOF mass and UV-vis spectra. $Fe_2$DTPFPP dimer shows peaks at $m/z$ values of 1798.4 corresponding to $Fe_2$DTPFPP (calcd. 1798.73) and 1834.0 corresponding to [$Fe_2$DTPFPP]Cl (calcd. 1834.18). $Fe_2DTF_2PP$ dimer shows peaks at $m/z$ values of 1474.5 corresponding to $Fe_2DTF_2PP$ (calcd. 1474.9). $Fe_2DTCl_2PP$ dimer shows only one peak of $m/z$ value of 1672.2 corresponding to $Fe_2DTCl_2PP$ (calcd. 1672.36). The $Fe_2$DTPP dimer shows peaks at $m/z$ values of 1294.1 corresponding to [$Fe_2$DTPP]Cl (calcd. 1294.47) and 1259.0 corresponding to $Fe_2$DTPP (calcd. 1259.02). $Fe_2$TPFPP-TMP shows peaks at $m/z$ = 1690.1 and 1655.0 corresponding to [$Fe_2$TPFPP-TMP]Cl (calcd. 1690.57) and $Fe_2$(TPFPP-TMP) (calcd. 1655.1). Figure S1 (SI) depicts the MALDI-TOF mass spectra of the six Fe-porphyrin dimers and their UV-vis spectra (15 μM) in DMF.

## References


1. Qiao, J., Liu, Y. Y., Hong, F. & Zhang, J. A review of catalysts for the electroreduction of carbon dioxide to produce low-carbon fuels. *Chem. Soc. Rev.* **43,** 631–675 (2014).
2. Costentin, C., Robert, M. & Saveant, J.-M. Catalysis of the electrochemical reduction of carbon dioxide. *Chem. Soc. Rev.* **42,** 2423–2436 (2013).
3. Lackner, K. S. A guide to $CO_2$ sequestration. *Science* **300,** 1677–1678 (2003).
4. Glasser, D., Hildebrandt, D., Liu, X., lu, X. & Masuku, C. M. Recent advances in understanding the Fischer–Tropsch synthesis (FTS) reaction. *Curr. Opin. Chem. Eng.* **1,** 296–302 (2012).
5. Martin, O. & Perez-Ramirez, J. New and revisited insights into the promotion of methanol synthesis catalysts by $CO_2$. *Catl. Sci. Technol*. **3,** 3343–3352 (2013).
6. Franke, R., Selent, D. & Börner, A. Applied hydroformylation. *Chem. Rev.* **112,** 5675–5732 (2012).
7. Hawecker, J., Lehn, J. M. & Ziessel, R. Electrocatalytic reduction of carbon dioxide mediated by Re(bipy)$(CO)_3$Cl (bipy = 2,2′-bipyridine). *J. Chem. Soc., Chem. Commun.* 328–330 (1984).
8. Machan, C. W. *et al.* Supramolecular assembly promotes the electrocatalytic reduction of carbon dioxide by Re(I) bipyridine catalysts at a lower overpotential. *J. Am. Chem. Soc.* **136,** 14598–14607 (2014).
9. Riplinger, C., Sampson, M. D., Ritzmann, A. M., Kubiak, C. P. & Carter, E. A. Mechanistic contrasts between manganese and rhenium bipyridine electrocatalysts for the reduction of carbon dioxide. *J. Am. Chem. Soc.* **136,** 16285–16298 (2014).
10. Vollmer, M. V. *et al.* Synthesis, spectroscopy, and electrochemistry of (α-diimine)M$(CO)_3$Br, M = Mn, Re, complexes: Ligands isoelectronic to bipyridyl show differences in $CO_2$ reduction. *Organometallics* **34,** 3–12 (2015).
11. Wong, K.-Y., Chung, W.-H. & Lau, C.-P. The effect of weak Brönsted acids on the electrocatalytic reduction of carbon dioxide by a rhenium tricarbonyl bipyridyl complex. *J. Electroanal. Chem.* **453,** 161–170 (1998).
12. Chen, Z. *et al.* Electrocatalytic reduction of $CO_2$ to CO by polypyridyl ruthenium complexes. *Chem. Commun*. **47,** 12607–12609 (2011).
13. Tamaki, Y., Morimoto, T., Koike, K. & Ishitani, O. Photocatalytic $CO_2$ reduction with high turnover frequency and selectivity of formic acid formation using Ru(II) multinuclear complexes. *Proc. Natl. Acad. Sci. USA* **109,** 15673–15678 (2012).
14. Ohtsu, H. & Tanaka, K. An organic hydride transfer reaction of a ruthenium NAD model complex leading to carbon dioxide reduction. *Angew. Chem. Int. Ed.* **51,** 9792–9795 (2012).
15. Tanaka, K. Metal-catalyzed reversible conversion between chemical and electrical energy designed towards a sustainable society. *Chem. Rec.* **9,** 169–186 (2009).
16. Kang, P. *et al.* Selective electrocatalytic reduction of $CO_2$ to formate by water-stable iridium dihydride pincer complexes. *J. Am. Chem. Soc.* **134,** 5500–5503 (2012).
17. Chen, Y., Li, C. W. & Kanan, M. W. Aqueous $CO_2$ reduction at very low overpotential on oxide-derived Au nanoparticles. *J. Am. Chem. Soc.* **134,** 19969–19972 (2012).
18. Zhu, W. *et al.* Monodisperse Au nanoparticles for selective electrocatalytic reduction of $CO_2$ to CO. *J. Am. Chem. Soc.* **135,** 16833–16836 (2013).
19. Costentin, C., Drouet, S., Robert, M. & Savéant, J.-M. A local proton source enhances $CO_2$ electroreduction to CO by a molecular Fe catalyst. *Science* **338,** 90–94 (2012).
20. Costentin, C., Drouet, S., Passard, G., Robert, M. & Savéant, J.-M. Proton-coupled electron transfer cleavage of heavy-atom bonds in electrocatalytic processes. Cleavage of a C-O bond in the catalyzed electrochemical reduction of $CO_2$. *J. Am. Chem. Soc.* **135,** 9023–9031 (2013).
21. Costentin, C., Passard, G., Robert, M. & Savéant, J.-M. Pendant acid–base groups in molecular catalysts: H-bond promoters or proton relays? mechanisms of the conversion of $CO_2$ to CO by electrogenerated iron(0)porphyrins bearing prepositioned phenol functionalities. *J. Am. Chem. Soc.* **136,** 11821–11829 (2014).
22. Costentin, C., Passard, G., Robert, M. & Savéant, J.-M. Ultraefficient homogeneous catalyst for the $CO_2$-to-CO electrochemical conversion. *Proc. Natl. Acad. Sci. USA* **111,** 14990–14994 (2014).
23. Costentin, C., Drouet, S., Robert, M. & Savéant, J.-M. Turnover numbers, turnover frequencies, and overpotential in molecular catalysis of electrochemical reactions. Cyclic voltammetry and preparative-scale electrolysis. *J. Am. Chem. Soc.* **134,** 11235–11242 (2012).
24. Beley, M., Collin, J. P., Ruppert, R. & Sauvage, J. P. Nickel(II)-cyclam: an extremely selective electrocatalyst for reduction of $CO_2$ in water. *J. Chem. Soc., Chem. Commun.* 1315–1316 (1984).

25. Beley, M., Collin, J. P., Ruppert, R. & Sauvage, J. P. Electrocatalytic reduction of carbon dioxide by by nickel cyclam$^{2+}$ in water: study of the factors affecting the efficiency and the selectivity of the process. *J. Am. Chem. Soc.* **108,** 7461–7467 (1986).
26. Froehlich, J. D. & Kubiak, C. P. Homogeneous $CO_2$ reduction by Ni(cyclam) at a glassy carbon electrode. *Inorg. Chem.* **51,** 3932–3934 (2012).
27. Bouttez, M., Molton, F., Chardon-Noblat, S. & Deronzier, A. [Mn(bipyridyl)$(CO)_3$Br]: an abundant metal carbonyl complex as efficient electrocatalyst for $CO_2$ reduction. *Angew. Chem. Int. Ed.* **50,** 9903–9906 (2011).
28. Sampson, M. D. *et al.* Manganese catalysts with bulky bipyridine ligands for the electrocatalytic reduction of carbon dioxide: eliminating dimerization and altering catalysis. *J. Am. Chem. Soc.* **136,** 5460–5471 (2014).
29. Thoi, V. S. & Chang, C. J. Nickel *N*-heterocyclic carbene–pyridine complexes that exhibit selectivity for electrocatalytic reduction of carbon dioxide over water. *Chem. Commun.* **47,** 6578–6580 (2011).
30. Appel, A. M. *et al.* Frontiers, opportunities, and challenges in biochemical and chemical catalysis of $CO_2$ fixation. *Chem. Rev.* **113,** 6621–6658 (2013).
31. Can, M., Armstrong, F. A. & Ragsdale, S. W. Structure, function, and mechanism of the nickel metalloenzymes, CO dehydrogenase, and acetyl-CoA synthase. *Chem. Rev.* **114,** 4149–4174 (2014).
32. Jeoung, J. H., Fesseler, J., Goetzl, S. & Dobbek, H. Carbon monoxide. toxic gas and fuel for anaerobes and aerobes: carbon monoxide dehydrogenases. In *Metal Ions in Life Sciences* Eds.: P. M. H. kroneck & M. E. Sosa Torres, Springer, Heidelberg, **14**, 37–69 (2014).
33. Ensign, S. A. Reactivity of carbon monoxide dehydrogenase from rhodospirillum rubrum with carbon dioxide, carbonyl sulfide, and carbon disulfide. *Biochemistry* **34,** 5372–5381 (1995).
34. Svetlitchnyi, V., Peschel, C., Acker, G. & Meyer, O. Two membrane-associated NiFeS-carbon monoxide dehydrogenases from the anaerobic carbon-monoxide-utilizing eubacterium Carboxydothermus hydrogenoformans. *J. Bacteriol.* **183,** 5134–5144 (2001).
35. Jeoung, J. H. & Dobbek, H. Carbon dioxide activation at the Ni,Fe-cluster of anaerobic carbon monoxide dehydrogenase. *Science* **318,** 1461–1464 (2007).
36. Fesseler, J., Jeoung, J.-H. & Dobbek, H. How the [$NiFe_4S_4$] cluster of CO dehydrogenase activates $CO_2$ and NCO. *Angew. Chem. Int. Ed.* **54,** 8560–8564 (2015).
37. Collin, J.-P., Jouaiti, A. & Sauvage, J.-P. Electrocatalytic properties of (tetraazacyclotetradecane)nickel(2+) and $Ni_2$(biscyclam)$^{4+}$ with respect to carbon dioxide and water reduction. *Inorg. Chem.* **27,** 1986–1990 (1988).
38. de Alwis, C. *et al.* Cyclic voltammetry study of the electrocatalysis of carbon dioxide reduction by bis(polyazamacrocyclic) nickel complexes. *Electrochimica Acta* **45,** 2061–2074 (2000).
39. Simon-Manso, E. & Kubiak, C. P. Dinuclear nickel complexes as catalysts for electrochemical reduction of carbon dioxide. *Organometallics* **24,** 96–102 (2005).
40. Haines, R. J., Wittrig, R. E. & Kubiak, C. P. Electrocatalytic reduction of carbon dioxide by the binuclear copper complex [$Cu_2$(6-(diphenylphosphino-2,2′-bipyridyl)$_2$$(MeCN)_2$][$PF_6$]$_2$. *Inorg. Chem.* **33,** 4723–4728 (1994).
41. Cheng, S. C., Blaine, C. A., Hill, M. G. & Mann, K. R. Electrochemical and IR spectroelectrochemical studies of the electrocatalytic reduction of carbon dioxide by [$Ir_2$(dimen)$_4$]$^{2+}$ (dimen = 1,8-Diisocyanomenthane). *Inorg. Chem.* **35,** 7704–7708 (1996).
42. Raebiger, J. W. *et al.* Electrochemical reduction of $CO_2$ to CO catalyzed by a bimetallic palladium complex. *Organometallics* **54,** 3345–3351 (2006).
43. Ratliff, K. S., Lentz, R. E. & Kubiak, C. P. Carbon dioxide chemistry of the trinuclear complex [$Ni_3$($\mu_3$-CNMe)($\mu_3$-I)(dppm)$_3$][$PF_6$]. Electrocatalytic reduction of carbon dioxide. *Organometallics* **11,** 1986–1988 (1992).
44. Lee, E. Y., Hong, D., Park, W. H. & Suh, M. P. Synthesis, properties, and reactions of trinuclear macrocyclic nickel(II) and nickel(I) Complexes: electrocatalytic reduction of $CO_2$ by nickel(II) Complex. *Eur. J. Inorg. Chem.* 3242–3249 (2003).
45. Rail, M. D. & Berben, L. A. Directing the reactivity of [$HFe_4N(CO)_{12}$]$^-$ toward $H^+$ or $CO_2$ reduction by understanding the electrocatalytic mechanism. *J. Am. Chem. Soc.* **133,** 18577–18579 (2011).
46. Tezuka, M. *et al.* Electroreduction of carbon dioxide catalyzed by iron-sulfur cluster compounds [$Fe_4S_4$(SR)$_4$]$^{2-}$. *J. Am. Chem. Soc.* **104,** 6834–6836 (1982).
47. Nakazawa, M. *et al.* Electrochemical reduction of carbon dioxide using iron–sulfur clusters as catalyst precursors. *Bull. Chem. Soc. Jpn.*, **59,** 809–814 (1986).
48. Yuhas, B. D., Prasittichai, C., Hupp, J. T. & Kanatzidis, M. G. Enhanced electrocatalytic reduction of $CO_2$ with ternary Ni-$Fe_4S_4$ and Co-$Fe_4S_4$-based biomimetic chalcogels. *J. Am. Chem. Soc.* **133,** 15854–15857 (2011).
49. Mohamed, E. A., Zahran, Z. N. & Naruta, Y. Efficient electrocatalytic $CO_2$ reduction with a molecular cofacial iron porphyrin dimer. *Chem. Commun.* **51,** 16900–16903 (2015).
50. Andrieux, C. P. & Savéant, J. M. Electrochemical reactions, In *Investigation of Rates and Mechanisms of Reactions*, Bernasconi, C. F. Ed. *Techniques of Chemistry*, Vol. 6, 41E, Part 2, pp. 305–390, Wiley: New York (1986).
51. Leitner, W. The coordination chemistry of carbon dioxide and its relevance for catalysis: a critical survey. *Coord. Chem. Rev.* **153,** 257–284 (1996).
52. Naruta, Y., Sasayama, M.-A. & Sasaki, T. Oxygen Evolution by Oxidation of Water with Manganese Porphyrin Dimers. *Angew. Chem. Int. Ed.* **33,** 1839–1841 (1994).
53. Shimazaki, Y. *et al.* Characterization of a dinuclear $Mn^V=O$ complex and its efficient evolution of $O_2$ in the presence of water. *Angew. Chem. Int. Ed.* **43,** 98–99 (2004).
54. Naruta, Y. & Sasayama, M. Importance of Mn–Mn separation and their relative arrangement on the development of high catalase activity in manganese porphyrin dimer catalysts. *J. Chem. Soc., Chem. Commun.* 2667–2668 (1994).
55. Osuka, A., Nakajima, S., Nagata, T., Maruyama, K. & Toriumi, K. A 1,2-Phenylene-Bridged Porphyrin Dimer-Synthesis, Properties, and Molecular Structure. *Angew. Chem. Int. Ed.* **30,** 582–584 (1991).


## Acknowledgements

Y.N. acknowledges the financial supports from JST ACT-C, JSPS KAKENHI Grant Numbers 23245035, 15K12720, and a Chubu University Research Grant.

## Author Contributions

Z.N.Z. and E.A.M. prepared and characterized the catalysts. Z.N.Z. did the electrocatalytic investigation and wrote the manuscript. Y.N. supervised the work.

## Additional Information

**Supplementary information** accompanies this paper at http://www.nature.com/srep

**Competing financial interests:** The authors declare no competing financial interests.

**How to cite this article**: Zahran, Z. N. *et al.* Bio-inspired cofacial Fe porphyrin dimers for efficient electrocatalytic $CO_2$ to CO conversion: Overpotential tuning by substituents at the porphyrin rings. *Sci. Rep.* **6**, 24533; doi: 10.1038/srep24533 (2016).